sustainable chemistry

MDPI

Article

Sustainable Production of Chitin Nanowhiskers from Crustacean Biomass Using Cost-Effective Ionic Liquids: Strategies to Avoid Byproduct Formation

Alexander S. Shkuratov [1,†], Reshma Panackal Shibu [1,†], Obste Therasme [2], Paula Berton [3,*] and Julia L. Shamshina [1,*]

[1] Fiber and Biopolymer Research Institute, Department of Plant and Soil Science, Texas Tech University, Lubbock, TX 79409, USA; alexshku@ttu.edu (A.S.S.); rpanacka@ttu.edu (R.P.S.)
[2] Department of Sustainable Resources Management, State University of New York College of Environmental Science and Forestry, Syracuse, NY 13210, USA; otherasm@esf.edu
[3] Chemical and Petroleum Engineering Department, University of Calgary, Calgary, AB T2N 1N4, Canada
* Correspondence: paula.berton@ucalgary.ca (P.B.); jshamshi@ttu.edu (J.L.S.)
† These authors contributed equally to this work.

Abstract: Nanochitin, especially in the form of chitin nanowhiskers (ChNWs), represents a significant advance in biopolymer technology due to its high specific surface area, superior tensile strength, and excellent thermal stability. Derived from crustacean waste, which contains 15–40% of chitin, these materials provide a sustainable option that diverts waste from landfills and contributes to environmental conservation. Traditional methods of isolating nanochitin are energy-intensive and generate substantial waste. This study introduces a more sustainable method using inexpensive ionic liquids (ILs) such as [Hmim][HSO_4] and [HN_{222}][HSO_4], which bypass the costly and destructive steps of traditional procedures. This study also identified the byproduct in IL-mediated chitin hydrolysis reaction as calcium sulfate dihydrate and presented a solution to circumvent the byproduct formation. The effectiveness of the [HN_{222}][HSO_4] IL in producing ChNWs from both purified chitin and crustacean biomass was assessed, showing a high yield and maintaining the purity and structural integrity of chitin, thereby demonstrating a significant reduction in the environmental footprint of ChNW production.

Keywords: chitin nanowhiskers; crustacean biomass; ionic liquids; gypsum formation

Citation: Shkuratov, A.S.; Panackal Shibu, R.; Therasme, O.; Berton, P.; Shamshina, J.L. Sustainable Production of Chitin Nanowhiskers from Crustacean Biomass Using Cost-Effective Ionic Liquids: Strategies to Avoid Byproduct Formation. *Sustain. Chem.* **2024**, *5*, 130–148. https://doi.org/10.3390/suschem5020010

Academic Editors: Domenico Licursi, Juan Hernández Adrover and Francisco José Hernández Fernández

Received: 20 April 2024
Revised: 24 May 2024
Accepted: 30 May 2024
Published: 3 June 2024

1. Introduction

Nanochitin, i.e., chitin in its nanostructure form, is considered to be one of the important biopolymeric nanomaterials due to its high specific surface area, high tensile strength, and thermal stability, as well as renewability and abundance [1]. Chitin is an abundant biopolymer [2] made of repeating 2-(acetylamino)-2-deoxy-D-glucose β-linked units [3], and is found in the shells of arthropods (crabs, lobster, and shrimps), the cell walls of fungi, insect cuticles (e.g., fly larvae), some mushrooms, and yeasts [4].

Nanochitin particles, also called chitin nanowhiskers (ChNWs), possess a specific stiffness (105 GPa g^{-1} cm^{-3}) that is larger than that of ceramics, metals, and even Kevlar®, suggesting their use for fabricating exceptionally strong materials. In addition, these particles are lightweight (with a density of 1.425 g cm^{-3}) [5], transparent, and have high longitudinal elastic modulus (theoretical value > 150 GPa) [5–7]. Nanochitin is mostly used as a reinforcement filler to enhance the strength and durability of synthetic plastics [8–12]. Its reinforcing ability is attributed to the formation of a hydrogen-bonded percolated network within the synthetic polymer matrix. Other applications of nanochitin include packaging replacements [13–15], cement additives [16,17], personal care, hygiene, and cosmetics [5], medical devices [18–21], filtration membranes [22–24], and flexible electronics [25–28].

Crustacean waste biomass is, by far, the most abundant source of chitin and contains 15–40% of this polymer [29,30]. Crustacean waste is considered an environmental hazard [31] since it is either dumped back into the ocean or disposed of in landfills. Using chitinous waste to manufacture chitinous products keeps waste out of landfills, benefits the environment, conserves resources, and provides additional revenue to agricultural and aquacultural businesses. However, the recovery of "bulk" chitin is challenging due to the chitinous matrix structure, which contains strong covalent and hydrogen bonds between layers of proteins (20–40%) and chitin. In addition, crustacean waste is also rich in minerals (20–50%).

To obtain nanochitin from biomass, conventional methods include two steps. The first step aims to recover chitin as pure as possible from the shell matrix. However, this initial step is destructive, wasteful, and energy-demanding since it involves deproteinization to remove proteins present in a shell matrix (using bases, e.g., NaOH) and, in the case of crustacean biomass, demineralization to remove minerals (using acids, e.g., HCl). Bleaching/discoloration is often required [32,33]. The process is conducted at relatively high temperatures (60–100 °C), and for a long time [34,35], utilizing ~1.2 kWh of electricity and generating > 500 L acidic and basic aqueous waste per 1 kg of "bulk" chitin.

In the second step, the hydrolysis of glycosidic bonds releases nanochitin particles from the "bulk" chitin [36–39]. Hydrochloric acid [36,37,39,40], sulfuric acid [41,42], 2,2,6,6-tetramethylpiperidine-1-oxyl radical (TEMPO)-mediated oxidation [43–45], periodate-mediated oxidation [46], ammonium persulfate-mediated oxidation [47], and Deep Eutectic Solvent systems [48] have been proposed for hydrolysis. For the overall 'traditional' process of obtaining chitin nanowhiskers, 74.6% of CO_2 footprint (677 kg CO_2 equiv.) comes from the chitin isolation itself, while only a quarter of its CO_2 footprint (229.8 kg CO_2 equiv.) comes from the nanowhisker production step [49]. Bypassing the first step could lower the environmental impact by 75% and address a critical sustainability gap in the preparation of chitin nanomaterials.

A dual catalyst–solvent treatment of biomass with 1-butyl-3-methylimidazolium hydrogen sulfate ([C_4mim][HSO_4]) recently showed the potential of this IL to bypass the first step of "bulk" chitin isolation in producing nanowhiskers [50,51]. In this process, biomass was pretreated with the IL and hydrolyzed in an IL–water (3:1) mixture. After quenching the reaction, the thick white gel-looking suspension was ultrasonicated, centrifuged, washed, and lyophilized. The overall mass yield of nanofillers was 79%, much higher than that reported for HCl hydrolysis (45–55%). No deacetylation took place during the treatment, and the degree of acetylation (%DA) was the same as that of commercial chitin.

Despite all its advantages and potential applications in biomass processing, [C_4mim][HSO_4] is costly, mainly due to its manufacturing method. The method involves the formation of 1-butyl-3-methylimidazolium bromide ([C_4mim]Br) by adding butyl bromide to methylimidazole, followed by an anion exchange process with sodium hydrogen sulfate [52–55]. Factors that add to the high cost include the limited sizes of ion-exchange columns and high resource (i.e., resin and solvent) consumption. In addition, this is a traditional batch process and not a continuous manufacturing.

Since IL cost, biomass load, and IL recovery are three parameters likely to exert a significant influence on the final cost of chitin nanowhiskers [56], the manufacturing scale synthesis of the ILs must not only utilize inexpensive reagents but also be simple, straightforward, and easily scalable. The first study that evaluated the costs of hydrogen sulfate-based ILs on a bulk scale was conducted by Chen et al. [57]. The study considered factors such as raw material cost, other operating costs (salary/wages), utility costs (e.g., electricity and cooling water), and wastewater treatment [58,59]. It was found that the ILs triethylammonium hydrogen sulfate ([HN_{222}][HSO_4]) and methylimidazolium hydrogen sulfate ([Hmim][HSO_4]) are significantly cheaper than [C_4mim][HSO_4], within a price range for typical organic solvents (USD 1.44–1.56 kg^{-1}) [57]. In this work, we assess the effectiveness of these cost-effective ILs (Figure 1) for isolating chitin nanowhiskers from

both purified chitin and crustacean biomass and evaluate the properties of the resultant materials.

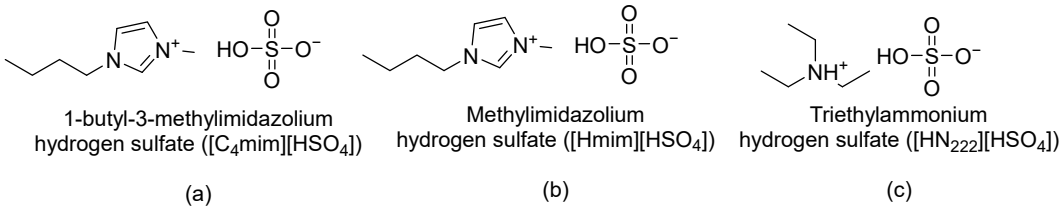

Figure 1. Ionic liquids used in this study: (**a**) 1-butyl-3-methylimidazolium hydrogen sulfate ([C_4mim][HSO_4]); (**b**) methylimidazolium hydrogen sulfate ([Hmim][HSO_4]); and (**c**) triethylammonium hydrogen sulfate ([HN_{222}][HSO_4]).

2. Materials and Methods

2.1. Materials

Commercial grade (purified) chitin, provided by Sigma-Aldrich (cat no: C7170, St. Louis, MO, USA) and Fisher Scientific (cat no: AAJ6120622, Hampton, NH, USA), was dried in an oven at 50 °C for 12 h before use. Crustacean (shrimp shells, SS, USA) biomass containing 24% chitin was obtained from Mari Signum, LLC (Richmond, VA, USA). To facilitate the extraction, the shells were washed, dried (50 °C for 12 h), ground, and sifted to achieve a particle size of less than 125 µm. The IL [Hmim][HSO_4] was purchased from Sigma-Aldrich (cat no: 59760, St. Louis, MO, USA) and [C_4mim][HSO_4] was purchased from Proionic (Graz, Austria), while [HN_{222}][HSO_4] was synthesized as previously reported [60,61]. Deionized water was bought from Aqua One (Amarillo, TX, USA). The calibration curve for the determination of the degree of acetylation (%DA) was constructed using chitosan from shrimp shells obtained from Sigma Aldrich (cat. No: C3646, St. Louis, MO, USA) with %DA = 30.0%, chitosan from shrimp shells obtained from Vanson HaloSource (cat. No: VNS-389, Redmond, WA, USA) with %DA = 23.9%, chitosan from Alfa Aesar (cat. No: J64143, Haverhill, MA, USA) with %DA = 15.0%, and chitin from Spectrum (cat. No: C2020, Gardena, CA, USA) with %DA = 86.0%.

2.2. Determination of Chitin Content in Biomass

The Black and Schwartz method was used to determine the amount of chitin in biomass [62]. Ground and sieved crustacean biomass (1 g) was weighed into a 50 mL round bottom flask equipped with a Teflon-coated magnetic stir bar and a condenser. Then, 24 mL of 1 M HCl was added and the mixture was heated under reflux with stirring at 750 rpm for 1 h. After 1 h, the flask was removed from heat and cooled to room temperature. The reaction mixture was transferred to a centrifuge tube and centrifuged at 3750 rpm for 10 min in a Beckman Coulter Allegra X-15R Refrigerated Centrifuge (Beckman, Brea, CA, USA). Then, the supernatant was carefully separated from the solids, 25 mL of fresh DI water was added, and the resultant suspension was centrifuged again. Centrifugation, aqueous phase decantation, and fresh DI water addition steps were consecutively repeated until the washings were no longer acidic. The remaining solid was transferred to its initial (water-rinsed) round bottom flask now with 24 mL of 1.25 M aqueous NaOH, and the mixture was heated under reflux with stirring at 750 rpm for 1 h. After 1 h, the reaction was once again removed from heat, cooled down and its content transferred to new centrifuge tubes, and centrifuged for 10 min at 3800 rpm. The supernatant was decanted and discarded, and the remaining solid was washed with the addition of fresh DI water, followed by centrifugation, again at 3750 rpm, for 10 min. The solid was repeatedly washed and centrifuged with fresh DI water (8 more times) until the supernatant was neutral. When the supernatant was neutral, it was decanted and discarded, and the remaining solid was transferred onto a Petri dish and dried overnight in an 80 °C Cole-Parmer StableTemp gravimetric convection oven (Charleston, SC, USA), and weighed to obtain the percent of chitin from biomass. The determination of chitin content was carried out in triplicate.

2.3. Preparation of Chitin Nanowhiskers

Chitin nanowhiskers were obtained by following the reported method (Figure S1, ESI) [50,51].

1. **Pretreatment with ILs**—For chitin pretreatment, a suspension of chitin in IL (1:10 w/w) was prepared by thoroughly mixing chitin in the IL (for example, 0.76 g chitin was added and mixed in 7.64 g $[HSO_4]^-$-based IL), resulting in a well-blended paste. The prepared paste was then properly sealed, encased with a parafilm, and kept in the oven (45–65 °C) for 24 h.
   For biomass pretreatment, a 3 wt% crushed crustacean biomass was prepared by thoroughly mixing the biomass in the IL (for example, 1.5 g crushed crustacean biomass was added and mixed in 48.5 g of the $[HSO_4]^-$-based IL), resulting in a paste. The properly blended paste was subsequently sealed, covered with a parafilm, and kept in the oven (45–65 °C) for 24 h.
2. **Isolation of Chitin Nanowhiskers**—After letting the mixture in the containers settle for 24 h, 30% DI water with respect to IL (i.e., 16.7 g of water per 48.5 g of the IL) was added to each flask. Each flask was equipped with a stirring bar and a condenser, and then heated to 110 °C in an oil bath, for 6–48 h. In the case of biomass, this resulted in a significant production of foam. After heating, 50 mL DI water was added to each flask. Following that, the mixtures were moved to 15 mL centrifuge tubes, and centrifuged (Eppendorf 5430 R, Enfield, CT; rotor CE 11017, 7830 rpm). The liquid was decanted, fresh water was added, the precipitate was stirred with a spatula, and the suspension was centrifuged again. This process was repeated 10 more times until a neutral pH was obtained. After washing, the suspensions were ultrasonicated (VibraCell Ultrasonicator, model CV 33, Newtown, CT, USA) for 10 min with 30 s cycles for the uniform distribution of particles. The suspension was then split into 2 parts. One part was diluted and analyzed using Transmission Electron Microscopy (TEM, Hitachi H-9500, Tokyo, Japan). The second part was frozen at −20 °C, and then subjected to a lyophilization (Labconco FreeZone Plus Cascade Benchtop Freeze Dryer System, Kansas City, MO, USA) process for approximately 72 h, resulting in the production of nanocrystals with precise dimensions.

2.4. Characterization

2.4.1. Estimation of Crystallinity

The crystallinity of the nanocrystals generated directly from crustacean biomass was measured using a powder X-ray diffractometer (HD 2711N, Rigaku, Tokyo, Japan) with Ni-filtered Cu Kα radiation and λ = 1.542 Å, at 44 mA and 40 kV. Diffractograms were collected under a scanning rate of 1° min^{-1} over the 2θ region ranges from 5 to 50°. Origin software (OriginLab Corporation, Northampton, MA, USA) was used for removing the background, and then for the smoothening and baseline correction of the recorded data. The Peak Analyzer tool was employed to automatically identify and analyze a wide range of multiple peaks, and the crystallinity of the product was finally computed using the equation:

$$CrI\ (\%) = \frac{\sum area\ of\ crystalline\ peaks}{\sum area\ of\ crystalline\ peaks\ and\ amorphous\ scattering} \times 100 \quad (1)$$

2.4.2. Crystallite Size Determination

The crystallite size was calculated using the Scherrer equation [63], previously employed for chitin [64]:

$$\beta = (k \times \lambda)/(L \times \cos(\theta)) \quad (2)$$

where β represents the crystallite size perpendicular to the lattice plane represented by (020) and (110) peaks, k is the Scherrer constant for a given crystal shape (k = 0.91), λ represents the wavelength of the incident X-rays (1.54 Å), L represents the width of the peak at half

of its maximum in radians (FWHM), and θ is the position of the peak (half of the plotted 2θ value).

2.4.3. Transmission Electron Microscopy

The morphology, including the distribution of nanocrystals (diluted 30-fold before analysis), size, and shape, was evaluated using a Transmission Electron Microscope (Hitachi H-9500, Tokyo, Japan).

2.4.4. Field Emission Scanning Electron Microscopy

A field emission scanning electron microscope (FE-SEM, S/N 4300, Hitachi, Chiyoda, Tokyo, Japan) was used for the visualization of gypsum crystals. For this, the samples were mounted on the sample stage with adhered carbon tape (Ted Pella Inc., Redding, CA, USA) and visualized at 500–5000 magnification, with an accelerating voltage of 15,000 V. Quartz PCI Imaging software (Version 8, Quartz Imaging Corp., Vancouver, BC, Canada) (https://www.quartzimaging.com/pci-microscope-imaging-software.html, accessed on 1 April 2024) was used to analyze the recorded images.

2.4.5. Thermal Gravimetric Analysis

The thermal stability of the generated nanocrystals was examined using a thermogravimetric analyzer (TGA, Pyris1, PerkinElmer Inc., Shelton, CT, USA). The samples were kept under controlled conditions at a temperature of 21 ± 1 °C with a relative humidity (RH) of 65 ± 2% before analysis. An inert atmosphere was maintained by flowing nitrogen at a rate of 20 mL min^{-1}. The thermal analysis was carried out at a heating rate of 10 °C min^{-1}, spanning the temperature range of 40 to 600 °C. The data generated were analyzed with the assistance of Pyris software (PerkinElmer Inc., Shelton, CT, USA).

2.4.6. Attenuated Total Reflectance (ATR) Fourier-Transform Infrared Spectroscopy (FTIR)

The structural characterization of the isolated nanocrystals was confirmed using an ATR FTIR Spectrum-400 instrument (PerkinElmer, Waltham, MA, USA). The samples were kept under controlled conditions at a temperature of 21 ± 1 °C with an RH of 65 ± 2% and then placed on a chemically inert Zn-Se-diamond crystal stage for analysis. A total of 64 scans were conducted, covering the spectral range from 650 to 4000 cm^{-1}, and the spectral resolution was set at 4 cm^{-1}. The results were recorded and interpreted with the aid of OPUS Bruker software (Bruker, Billerica, MA, USA).

2.4.7. Degree of Acetylation

FTIR spectroscopy was employed to assess the degree of acetylation (%DA) of the chitin nanocrystals, following the same procedure detailed by Beil et al. [65]. First, the calibration curve was constructed as follows. The ATR FTIR spectra (64 scans) were recorded for chitin and chitosan with known %DA (15, 24, 30, and 86%). The spectra were converted to Transmittance, then smoothed employing a 9-point Savitzky–Golay algorithm, and the first derivatives of the spectra were calculated. The first derivative ATR FTIR values at 1383 cm^{-1} (MB1), 1327 cm^{-1} (MB2), and 1163 cm^{-1} (RB) were determined and the ratios (MB1 + MB2)/RB were found. The data were then plotted as %DA vs. (MB1 + MB2)/RB. This calibration curve (Figures S2 and S3, ESI) was used to determine the %DA for prepared samples.

3. Results and Discussion

3.1. Preparation and Characterization of Chitin Nanowhiskers from Pure Chitin

Chitin nanowhiskers were prepared using cheaper [Hmim][HSO_4] and [HN_{222}][HSO_4] and compared side-by-side with those prepared using the more expensive IL [C_4mim][HSO_4] [50,51]. In addition to the price difference, [Hmim][HSO_4] and [HN_{222}][HSO_4] are defined as "protic" ILs, whose pKa values for cations are 6.95 and 10.72, respectively [66,67]. The IL [Hmim][HSO_4] was commercially available, whereas

$[HN_{222}][HSO_4]$ was prepared by mixing triethylamine with sulfuric acid through a simple Brønsted acid-base proton transfer reaction [60,61].

As an initial step, the ILs were tested for the preparation of ChNWs from pure chitin, to determine their ability to hydrolyze the glycosidic linkages (Figure S1, ESI). In brief, chitin was pretreated with $[C_4mim][HSO_4]$ (used as a benchmark) [50,51], [Hmim][HSO_4], or $[HN_{222}][HSO_4]$, for 24 h. Since the three ILs are solids at room temperature (with melting temperatures of 28.7 [68], 40.6 [69], and 85 °C [70] for $[C_4mim][HSO_4]$, [Hmim][HSO_4], and $[HN_{222}][HSO_4]$, respectively), the pretreatment temperature was kept higher than their melting points. After pretreatment, DI water was added and the solutions were heated to 110 °C for 48 h under reflux. The precipitate was centrifuged, washed with water, and ultrasonicated. The suspension was then split into two parts. One part was diluted and used for Transmission Electron Microscopy (TEM) imaging while the second one was dehydrated using freeze-drying and used for further characterization. Based on the IL used to prepare the ChNWs from chitin, the products were denoted as ChNWs/Ch/$[C_4mim][HSO_4]$, ChNWs/Ch/[Hmim][HSO_4], and ChNWs/Ch/$[HN_{222}][HSO_4]$. All the dried products appeared as white powders and similar yields, i.e., 54, 55, and 50%, were obtained for ChNWs/Ch/$[C_4mim][HSO_4]$, ChNWs/Ch/[Hmim][HSO_4], and ChNWs/Ch/$[HN_{222}][HSO_4]$, respectively. Such moderate yield was reported in the literature in other acidic systems, where the acidic hydrolysis of chitin leads to the formation of not only ChNWs but also chitin oligomers [71,72]. Decreasing the time to 24 h during subsequent studies produced the nanomaterial in the same yields.

The dimensional parameters of the ChNWs processed using each IL were obtained from TEM. A 10-times dilution of the original suspensions, obtained after ultrasonication, with a concentration of ~0.1 mg mL^{-1} was the most suitable for TEM imaging. As shown in the TEM images (Figure 2), the morphology of the nanowhiskers was highly regular. The ChNWs from [Hmim][HSO_4] and $[HN_{222}][HSO_4]$ presented elongated crystalline rod-like nanoparticles, characterized by pointed ends, with diameters ranging between 20 and 22 nm, and lengths ranging between 230 and 246 nm (Table 1). Given the obtained results, we estimated the average aspect ratio (L/d) to be ~12 to 12.5. These findings correlate with those previously reported when using $[C_4mim][HSO_4]$ for hydrolysis, with diameters of 21.7 ± 5.5 nm and lengths of 216 ± 78 nm. Overall, the ChNWs obtained showed a similar length and diameter, i.e., avg. 230 ± 12 nm and 21.3 ± 0.9 nm, respectively. For comparison, the aspect ratio of ChNWs obtained through hydrolysis with HCl can range from 15 to 120, depending on the chitin source used [73]. The size of ChNWs is directly dependent on the biomass it was isolated from. For example, the hydrolysis of α-chitin from shrimp shells using 3 N HCl results in nanowhiskers with an average length and width of 216 ± 91 nm and 16.4 ± 5.8 nm [74]. When chitin is sourced from *Riftia* tubes, the resulting ChNWs have a length range from 500 nm to a few μm [75]. The size of the nanowhiskers from Oyster and Button mushrooms ranging from 50 to 200 nm in length and ~11 nm in diameter [76].

Table 1. Dimensional parameters of the ChNWs isolated from chitin using different ILs.

ChNW Prepared from Chitin Hydrolyzed with	Yield %	Dimensions	Size (nm) Mean ± STD	Sample Size	Aspect Ratio Mean ± STD	Sample Size
$[C_4mim][HSO_4]$ *	54	Length	216 ± 78	72	11.0 ± 4.9	38
		Diameter	21.7 ± 5.5	38		
[Hmim][HSO_4]	55	Length	230 ± 84	65	12.5 ± 6.0	65
		Diameter	20.0 ± 7.7	79		
$[HN_{222}][HSO_4]$	50	Length	246 ± 89	94	12.1 ± 5.9	72
		Diameter	22.2 ± 5.9	72		

* Original study. All nanowhiskers prepared from pure chitin have approximately the same dimensions, i.e., 230 ± 12 nm in length and 21.3 ± 0.9 nm in diameter.

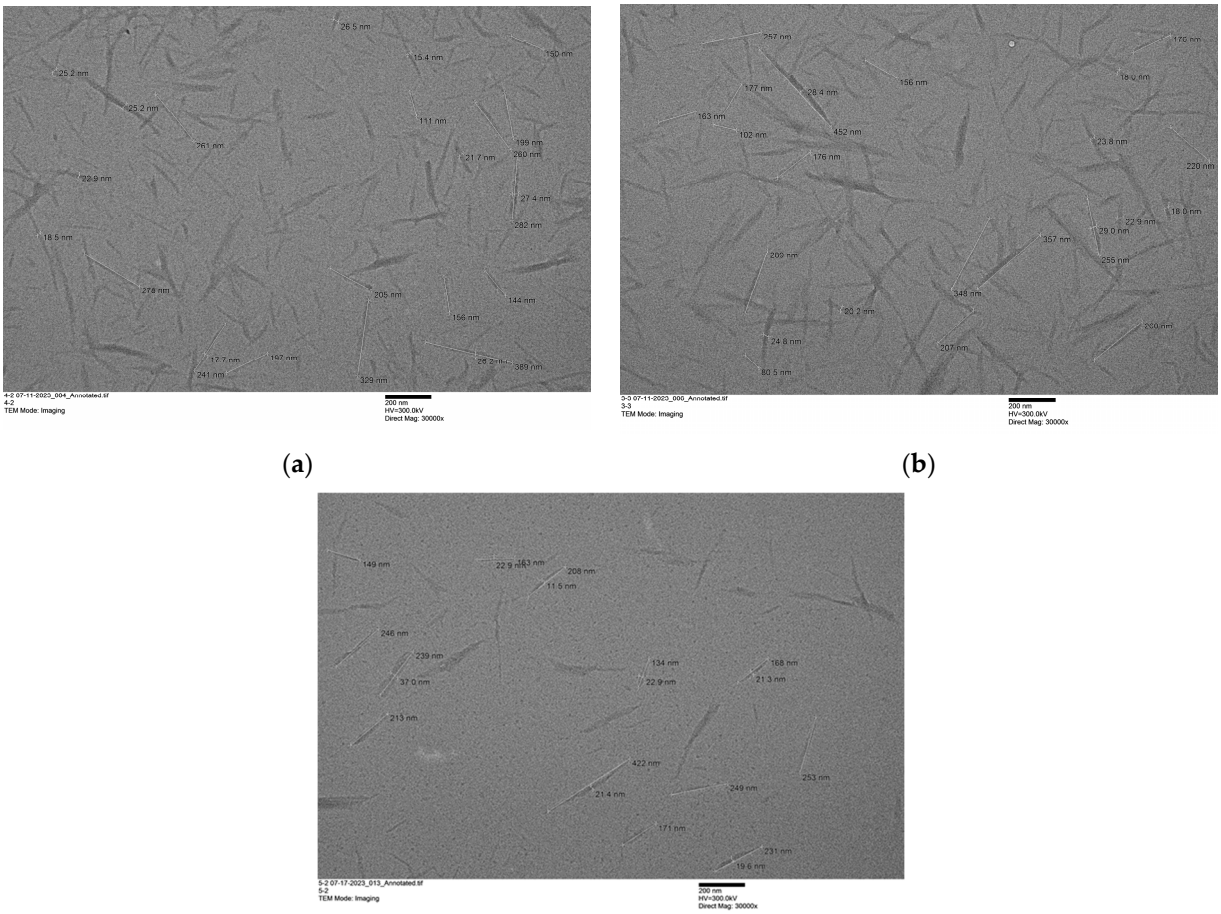

Figure 2. TEM micrograph of a dilute suspension of chitin nanowhiskers derived from purified chitin using (**a**) $[C_4mim][HSO_4]$, (**b**) $[Hmim][HSO_4]$, and (**c**) $[HN_{222}][HSO_4]$. HV 300 kV. Magnification: 30,000×; scale bar 200 nm.

Attenuated Total Reflectance (ATR) Fourier-Transform Infrared Spectroscopy (FTIR) was then used to detect chemical modifications to the chitin due to the IL treatment. The spectral peaks were compared with those identified in standard chitin reference upon the normalization of the FTIR spectra (Figure 3; expanded spectra of different FTIR regions are shown in Figures S4–S6, ESI). Independent of the IL used for hydrolysis, the obtained ChNW/Ch/ILs showed almost identical spectrum profiles (Figure 3). The spectra of ChNW/Ch/ILs were not only similar to each other but also to the spectrum of pure chitin that was used as the starting material and to those reported in the literature (summarized in Table S1, ESI). Thus, the peak attributed to O(3)H$\cdots$O(5) from the ring in the α-chitin was located at the same position in all ChNW/Ch/ILs and chitin standard, at 3438 cm^{-1}. The peaks were also of the same intensity, indicating no hydrolysis-induced changes in –O–H stretching. The same observation (i.e., peaks of close intensity situated at the same wavenumber for both ChNW/Ch/ILs products and pure chitin standard) is valid for the N–H stretching and bending, at 3103 cm^{-1} and 1556 cm^{-1}, respectively. Similarly, no differences were found in the location or intensity of Amide III peaks (namely, C–N and N–H) at 1311 cm^{-1} and N–H peak at 3261 cm^{-1}. Both the intensity and the wavenumber of the vibration modes of carbonyl (Amide I), namely, the C=O$\cdots$H–N vibration at 1654 cm^{-1} and the $–CH_2OH\cdots$O=C band at 1620 cm^{-1}, were also retained, indicating no changes in amide-type of hydrogen bonding. Concerning C–O, the stretching of glycosidic linkage (the asymmetric bridge oxygen stretching) is indicated by a peak at 1154 cm^{-1}, and pyranose ring stretching was found at 895 cm^{-1}.

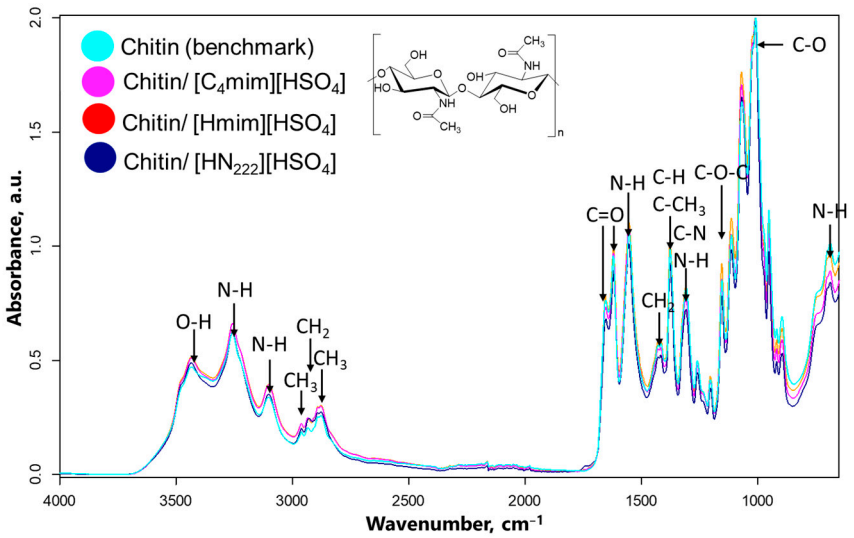

Figure 3. ATR FTIR spectra (4000–650 cm^{-1}) of chitin (aqua) and chitin nanowhiskers (ChNWs): ChNWs/Ch/[Hmim][HSO_4] (red), ChNWs/Ch/[HN_{222}][HSO_4] (blue), and ChNWs/Ch/[Hmim][HSO_4] (pink).

As for CH bonds, a symmetric stretching vibration of the CH_3 group from –NHC(O)CH_3 amide bond, a asymmetric stretching vibration of the CH_2 group from CH_2OH, and stretching vibrations of CH in the pyranose ring appeared at 2964, 2930, and 2886 cm^{-1}, respectively. The CH_3 deformation appeared at 1378 cm^{-1} in both standard and nanowhiskers, whereas –CH_2 ending in CH_2OH showed up at 1425 cm^{-1}. The bands at 970 cm^{-1} and 873 cm^{-1} correspond to vibrations of CH_3 wagging and the C–H vibrations of CH_3 in the ring structure. Overall, the obtained ChNW/Ch/ILs produced in this study did not indicate any significant change in chemical functional groups compared to the native chitin. This finding differs from what was shown before for acid hydrolysis [77], which reported that the use of an acidic environment leads to partial chitin deacetylation.

Powder X-ray diffraction (pXRD) was used to elucidate the degree of crystallinity of all products (Figure 4). For that, the diffractograms obtained for ChNW/Ch/ILs samples were compared with the diffractogram of pure chitin. In all diffractograms, the peaks were found at 9.24°, 12.69°, 19.23°, 20.58°, 23.18°, and 26.27°, corresponding to (0 2 0), (0 2 1), (1 1 0), (1 2 0), (1 3 0), and (0 1 3) reflections, respectively [78,79]. The crystallinity index (CrI) was determined using the peak height method based on a comparison of the intensity of a crystalline reflection 19.23° (I_{110}) and the height of amorphous scattering (16°, I_{am}) [80,81]. However, the reliability of this method is based on the precision of background subtraction and the presence of both anhydrous and hydrated polymorphs [82]. Therefore, we have also employed the peak deconvolution method that typically provides higher accuracy [83,84]. This method is based on calculating the ratio between the area of crystalline peaks and the total area of a pXRD pattern. Figures S8–S13 and Tables S2–S7 (ESI) provide the calculated peak fitting of the diffraction profiles, the calculated peak locations, areas under the peak, and full width at half maximum (FWHM) values.

While starting chitin was found to be 84% crystalline, the crystallinity values of ChNWs from [HN_{222}][HSO_4] was similar (84.5%), slightly lower for [Hmim][HSO_4] (79.8%), and significantly higher for the [C_4mim][HSO_4] IL (92.6%, Table 2). The crystallite size values (Tables 2, S8 and S9, ESI) were calculated using Scherrer's equation [63]. Specifically, the crystallite size (a measure of the coherent volume for chitin in the diffraction peak) of each type of nanowhiskers was determined for two of the most prominent crystalline peaks of chitin, at the (0 2 0) and (1 1 0) planes, and was found to be between 6.9 and 8.6 nm (at the (0 2 0) plane) and between 5.2 and 7.5 nm (at the (1 1 0) plane), consistent with those observed previously. Thus, nanowhiskers obtained using HCl-hydrolysis from crab chitin demonstrated a crystallinity index of 86%, whereas the crystallite dimensions at the (0 2 0)

and (1 1 0) planes for CtNWs were 9.2 nm and 6.5 nm, respectively [85]. Likewise, the acid hydrolysis of α-chitin from shrimp shells produced nanowhiskers with a crystallinity index of 93.6% and crystallite dimensions of 6.3 nm at the (1 1 0) plane [86]. However, since the peaks were not fitted most appropriately for detailed structural reporting (chi-squared in the range of 10^{-4}), it would be advisable that researchers use the crystallite size data with appropriate caution.

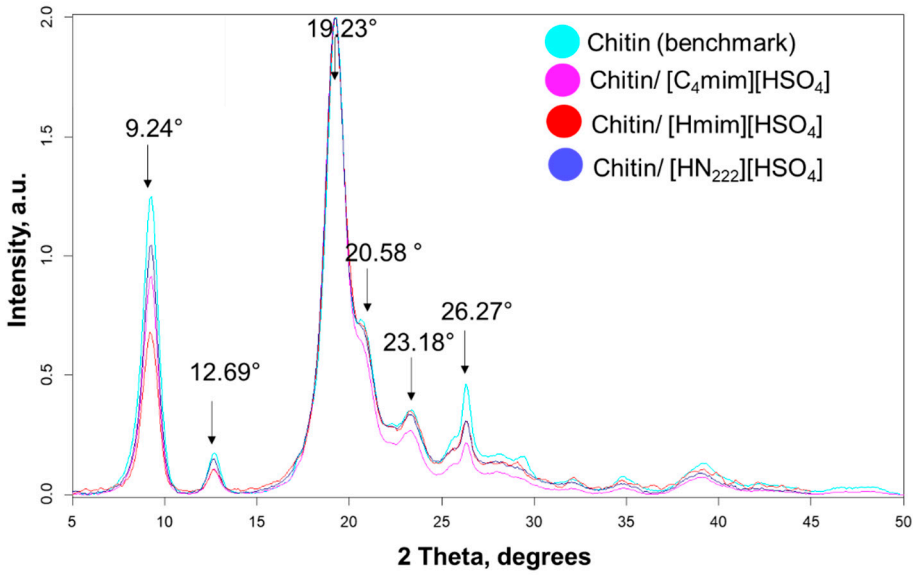

Figure 4. Full diffractograms (5–50° 2 Theta) of chitin (aqua) and chitin nanowhiskers (ChNWs): ChNWs/Ch/[Hmim][HSO_4] (red), ChNWs/Ch/[HN_{222}][HSO_4] (blue), and ChNWs/Ch/[Hmim][HSO_4] (pink).

Table 2. Crystallinity index (CrI, %) determined via peak height and peak deconvolution methods and crystallite size (nm) at the (0 2 0) and (1 1 0) planes.

	Crystallinity Index via Peak Height (CrI), %	Crystallinity Index via Deconvolution (CrI), %	Crystallite Size at the (0 2 0) Plane, nm	Crystallite Size at the (1 1 0) Plane, nm
Chitin Standard	98.0	84.0	6.9	5.2
ChNWs/Ch/[HN_{222}][HSO_4]	98.0	84.5	8.5	7.5
ChNWs/Ch/[Hmim][HSO_4]	98.0	79.8	8.1	5.8
ChNWs/Ch/[C_4mim][HSO_4]	98.1	92.6	8.6	6.3

The degree of acetylation (%DA) was also determined for pure chitin and all ChNWs/Ch/ILs, using the first derivative of FTIR spectra (Figure S13, Table S10, ESI), as reported by Beil et al. [65]. The technique compares the heights of the C–H deformation band (1383 cm^{-1}, MB1), the amide III band (1327 cm^{-1}, MB2), and the bridge oxygen stretching band (1163 cm^{-1}, RB) in the first derivative ATR FTIR spectra with those obtained for several external standards (chitins and chitosans with a known value of %DA). A calibration curve (also called a standard curve) was generated by plotting the value [(MB1 + MB2)/RB] against %DA for a series of reference standards. Back calculations using this calibration curve (Figure S2, ESI) revealed the %DA in the range of 97–100% in all cases.

3.2. Preparation and Characterization of Chitin Nanowhiskers from Crustaceous Biomass

As demonstrated in the previous section, all three ILs, i.e., [C_4mim][HSO_4], [Hmim][HSO_4], and [HN_{222}][HSO_4], were able to hydrolyze chitin and produced ChNWs with similar dimensions. These same ILs were then used to simultaneously pulp and hydrolyze crustacean biomass (shrimp shells, SS) using a two-step procedure, sim-

ilar to the one described for commercial chitin. Briefly, SS was first pretreated with $[C_4mim][HSO_4]$ [50,51], $[Hmim][HSO_4]$, or $[HN_{222}][HSO_4]$ for 48 h, followed by the addition of DI water and 110 °C heating under reflux for 48 h. In comparing the reactions between the ILs with the two starting materials (chitin or SS), it is worth noting that the reaction with SS proceeded much more vigorously than the same reaction with chitin, and created foam in all cases, likely due to the release of carbon dioxide from calcium carbonate ($CaCO_3$, present in the SS) under acidic conditions. After dilution with water, centrifugation, washing, and lyophilization, the product yield was 75–80% based on chitin available in the SS (Table 3), with yields significantly higher than those obtained from pure chitin.

Table 3. Dimensional parameters of the ChNWs isolated from shrimp shells (SS) using different ILs.

ChNW Prepared from SS Hydrolyzed with	Yield %	Dimensions	Size, nm Mean ± STD	Sample Size	Aspect Ratio Mean ± STD	Sample Size
$[C_4mim][HSO_4]$ *	75	Length	561 ± 157	36	55.5 ± 22.1	36
		Diameter	10.0 ± 3.6	90		
$[Hmim][HSO_4]$	80	Length	576 ± 168	21	55.2 ± 28.1	21
		Diameter	11.7 ± 2.9	62		
$[HN_{222}][HSO_4]$	79	Length	612 ± 198	41	34.8 ± 18.8	41
		Diameter	17.3 ± 3.9	127		

* Original study [50,51]. For comparison, all nanowhiskers prepared from biomass have approximately the same dimensions, i.e., 583 ± 21 nm in length and 21.3 ± 0.9 nm in diameter.

The analysis of TEM micrographs revealed that ChNWs from SS (sample ID ChNWs/SS/ILs, Figure 5) had a length ranging from 560 to 612 nm, i.e., roughly 2.5–3 times longer compared to ChNWs/Ch/ILs, and diameters ~10–20 nm (Table 3). When considering aspect ratios, calculated as the ratio of length to diameter (L/d), ChNWs/SS/ILs showed ~3–5 times larger aspect ratio than ChNWs/Ch/ILs. Interestingly, while ChNWs prepared using imidazolium ILs were ~2 times narrower in diameter than ChNWs/Ch/imidazolium ILs, ChNWs/SS/$[HN_{222}][HSO_4]$ showed a similar diameter as ChNWs/Ch/$[HN_{222}][HSO_4]$.

Upon examining the FTIR spectra (Figure 6) of the obtained ChNWs, it became evident that while the location and intensity of the peaks of ChNWs/SS/$[C_4mim][HSO_4]$ closely resembled those of commercially available chitin [50,51], there were significant differences in the spectra of ChNWs/SS produced using "inexpensive" ILs, i.e., ChNWs/SS/$[Hmim][HSO_4]$ or ChNWs/SS/$[HN_{222}][HSO_4]$. The spectrum of ChNWs/SS/$[Hmim][HSO_4]$ exhibited peaks typical for chitin; however, the intensities of many peaks were found to be somewhat greater than those typically associated with the biopolymer. This was particularly true for weak vibrations at 3483 and 3437 cm^{-1}, normally associated with water molecules, weak peaks in the region 820–650 cm^{-1}, and medium/strong vibrations at 1155 and 1116 cm^{-1}, characteristic of sulfate ion [87–89]. The FTIR spectrum of ChNWs/SS/$[HN_{222}][HSO_4]$ also showed peaks of enhanced intensities similar to the ones described for ChNWs/SS/$[Hmim][HSO_4]$. In this sample, additional peaks at 3152, 1555, 1401, 1170, and 974 cm^{-1} were identified, which did not match either chitin or sulfate (indicated in Figure 6a–d in blue color). The peaks did not belong to ionic liquids (Figure S7). We suggest that the reader consult the SI file, where the expansion of the FTIR regions is provided. Byproduct formation was reproducible in both cases.

Powder X-ray diffractograms (Figure 7) of ChNWs/SS/$[Hmim][HSO_4]$ and ChNWs/SS/$[HN_{222}][HSO_4]$ confirmed the presence of chitin (at 9.24°, 12.69°, 19.23°, 20.58°, 23.18°, and 26.27°, respectively [78,79]), but also peaks that did not belong to the biopolymer, at 11.56, 20.68, 23.33, and 29.07° 2θ. The amount of chitin was significantly greater in ChNWs/SS/$[HN_{222}][HSO_4]$, whereas ChNWs/SS/$[Hmim][HSO_4]$ showed a significant amount of byproduct. Interestingly, no byproduct formation was detected in ChNWs/SS/

$[C_4mim][HSO_4]$. It is also worth noting that the same byproduct was formed regardless of the "inexpensive" IL's identity, excluding any compound that could be derived from the ILs themselves. Also important is that the byproduct formed only in the case of IL reactions with biomass but was not seen when pure chitin polymer was hydrolyzed using these ILs, despite identical reaction conditions. This suggests that the formation of the byproduct had something to do with minerals present in biomass.

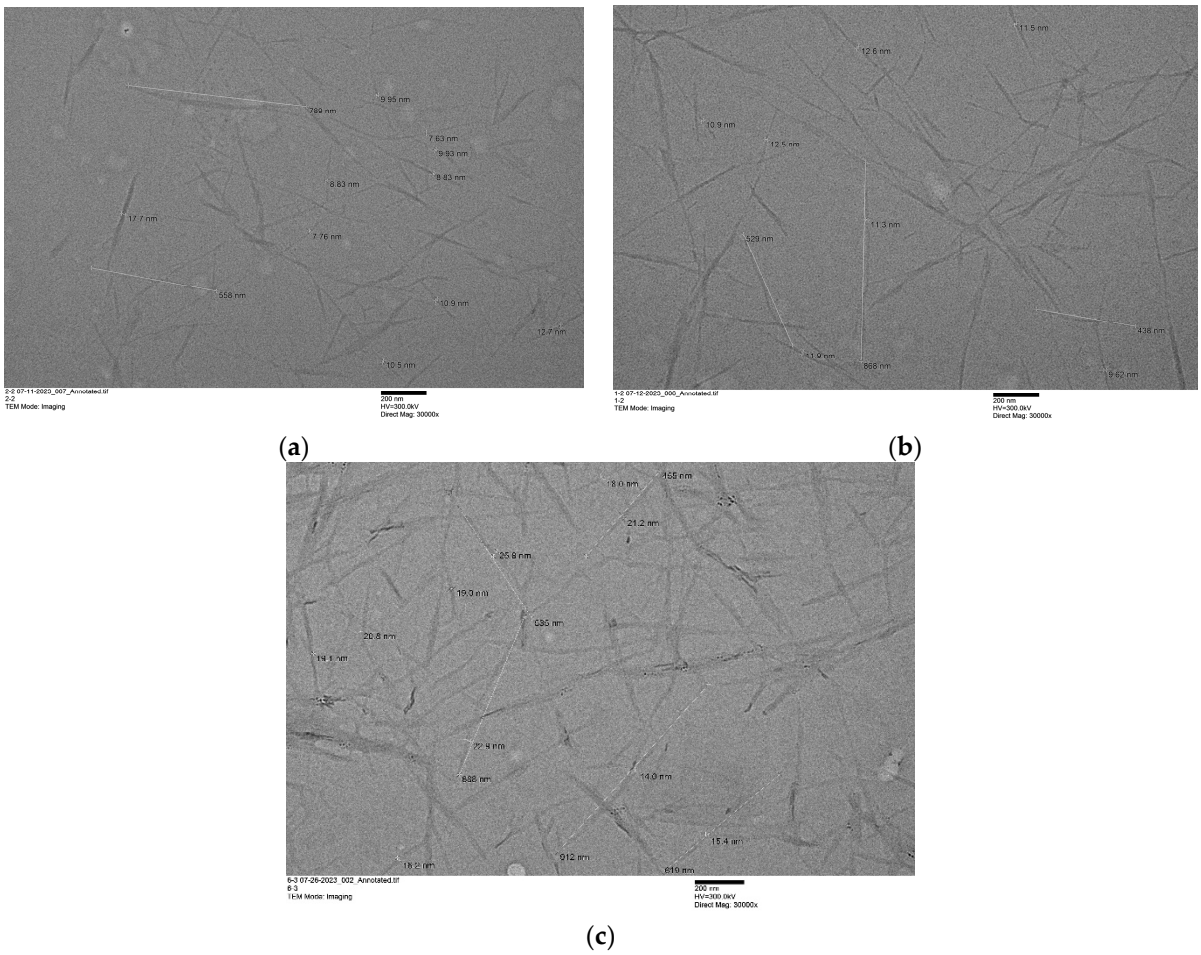

Figure 5. TEM micrograph of a dilute suspension of chitin nanowhiskers derived from purified chitin using (**a**) $[C_4mim][HSO_4]$, (**b**) $[Hmim][HSO_4]$, and (**c**) $[HN_{222}][HSO_4]$. HV 300 kV. Magnification: 30,000×; scale bar 200 nm.

Since one of the goals of this work was to generate high-purity chitin, identifying the new material was of great importance. An analysis of the literature identified the peaks at 11.56, 20.68, 23.33, and 29.07° 2θ as calcium sulfate dihydrate (also known as gypsum, $Ca(SO_4)\cdot 2H_2O$) [90]. TEM images did not show the presence of gypsum, likely because of the mineral being dissolved in water during the preparation of the sample for TEM analysis. On the other hand, lyophilized samples were expected to contain both chitin nanocrystals and gypsum after water removal. When the ChNWs/SS/$[HN_{222}][HSO_4]$ lyophilized sample was dispersed in a small amount of water and placed onto a carbon tape, followed by slow water evaporation, Scanning Electron Microscopy (SEM) imaging revealed the presence of gypsum crystals (Figure 8).

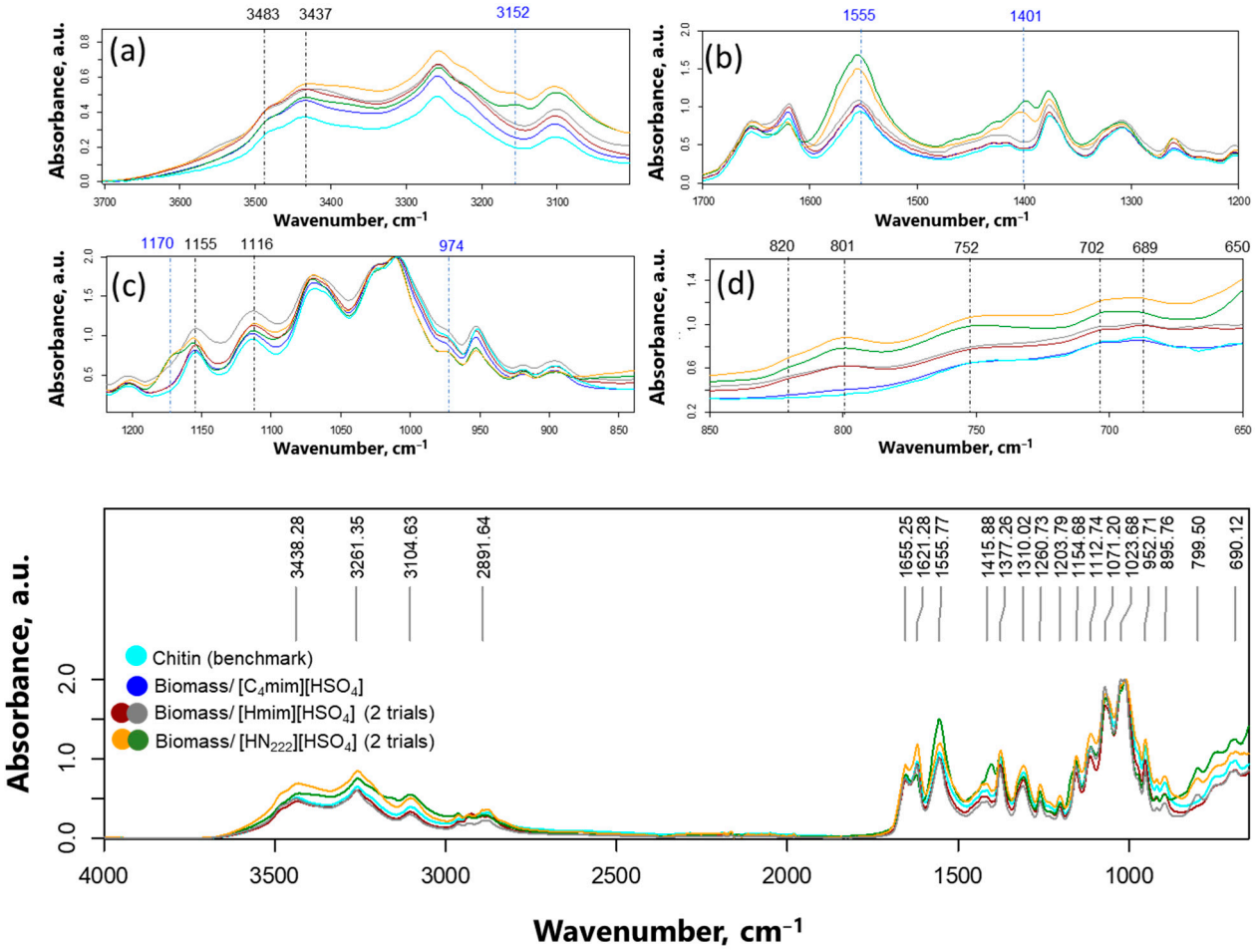

Figure 6. FTIR spectra of pure chitin (aqua) and chitin nanowhiskers (ChNWs) obtained from SS: ChNWs/SS/[C_4mim][HSO_4] (blue), ChNWs/SS/[Hmim][HSO_4] (brown and grey, two trials), and ChNWs/SS/[HN_{222}][HSO_4] (orange and green, two trials).

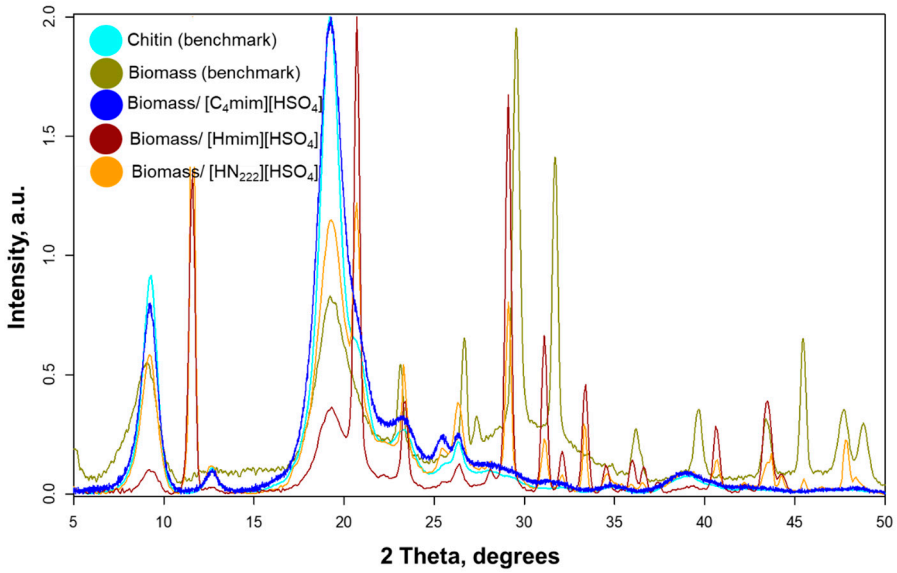

Figure 7. Diffractograms of pure chitin (aqua) and chitin nanowhiskers (ChNWs) obtained from shrimp shells: ChNWs/SS/[C_4mim][HSO_4] (blue), ChNWs/SS/[Hmim][HSO_4] (brown), and ChNWs/SS/[HN_{222}][HSO_4] (orange).

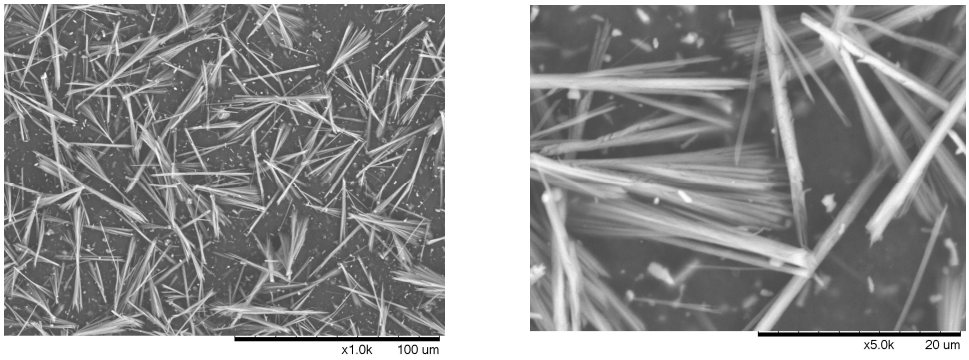

Figure 8. Gypsum crystals as obtained from biomass using [Hmim][HSO_4] and [HN_{222}][HSO_4] (left, right) looking identical to those provided in ref. [91]. No coating was used for imaging. Note that no ChNWs could be seen at this low magnification.

The reaction of acidic ILs with SS resulted in foam formation, which was attributed to CO_2 release from $CaCO_3$ in acidic conditions. This same reaction generates $CaSO_4$, which was previously reported to be ~5–10 times less soluble in the presence of 10% of alkylimidazolium hydrogen sulfate ILs than in pure water (0.055 mol/kg) [92], which would induce the coprecipitation of $CaSO_4$ together with ChNWs. However, a comparatively lesser decrease in the solubility of $CaSO_4{\cdot}2H_2O$ was observed for [C_4mim][HSO_4] when compared with [C_2mim][HSO_4], indicating an influence of the alkyl chain at the N2 atom of the imidazolium cation on the mineral's aqueous solubility [92]. With respect to the discussed reactions, no gypsum was detected when [C_4mim][HSO_4] was used to recover ChNWs from biomass, while a significant amount of gypsum was detected when [Hmim][HSO_4] was used. Considering that the difference between the ILs is only the butyl substituent on the N2 atom of imidazolium, we hypothesize that it is a protonated nitrogen atom of the cation of the IL that participates in the byproduct formation. The protonated ammonium or imidazolium could be stabilizing CO_3^{2-} from the $CaCO_3$ mineral of SS in solution through electrostatic interactions. It could also undergo deprotonation and react with CO_2 liberated by the reaction of $[HSO_4]^-$ with $CaCO_3$ with the formation of carbamates.

Regardless, the next step was adjusting the reaction conditions to minimize the formation of gypsum. Hence, the pretreatment step was eliminated. However, when SS was treated with [Hmim][HSO_4] without pretreatment, there still was a significant amount of gypsum present. Decreasing the reaction time first to 24 h, then to 12 h, and then to 6 h did not result in the removal of gypsum. Contrarily, the treatment of SS with [HN_{222}][HSO_4] provided a pure chitin product upon excluding the pretreatment step and reducing the reaction time to 24 h. Eliminating the pretreatment step aimed to remove the need for 24 h heating at 90 °C, leading to a favorable result.

The yield of the product decreased from 79 to 72%, whereas ChNWs' dimensions remained approximately the same (Table 4), not surprising considering that TEM imaging was only suitable for chitin visualization. The crystallinity, determined using the peak fitting method, was found to be 79.4%, a value very similar to that of ChNWs/SS/[C_4mim][HSO_4] (80.6%, Tables S8 and S9, ESI). The crystallite size was determined to be 7.1 nm at the (0 2 0) plane and 6.1 nm at the (1 1 0) plane (Table S9, ESI), also very close to that obtained for ChNWs/SS/[C_4mim][HSO_4] (8.4 and 5.6 nm at the (0 2 0) and (1 1 0) planes). The %DA calculated was found to be ~100%. Thermal analysis data have shown that $T_{50\%dec}$ was 341.7 °C, compared with 347 °C reported for pure chitin [93]. Overall, the [HN_{222}][HSO_4] IL performed very similarly to the [C_4mim][HSO_4] IL for biomass treatment and required milder reaction conditions, i.e., no pretreatment and 12 h reflux.

Table 4. Dimensional parameters of the ChNWs/SS/ILs without pretreatment step.

ChNW Prepared from Biomass Hydrolyzed with	Yield %	Dimensions	Size Mean ± STD	DA %	CrI %	Crystallite Size, nm	
						(0 2 0)	(1 1 0)
$[C_4mim][HSO_4]$ *	75	Length	561 ± 157	~100 [a]	80.6	8.4	5.6
		Diameter	10.0 ± 3.6				
$[HN_{222}][HSO_4]$	72	Length	588 ± 163	~100 [a]	79.4	7.1	6.1
		Diameter	17.1 ± 4.1				

* Original study [50,51]. [a] Calculated value is >100 (empirical method).

This innovative approach to producing ChNWs from crustacean biomass will contribute to advancing the circular economy concept. Crustacean biomass (e.g., shrimp shells) which would normally be sent to a waste treatment process (landfill) can be valorized through this process. Furthermore, the environmental impact of nanochitin production is considerably diminished through this method. By reducing hazardous chemical use and waste generation, the process aligns with global sustainability goals, notably cutting CO_2 emissions by approximately 75%.

To make sure that the process is environmentally viable, future research will perform an environmental life cycle assessment (LCA) The International Standardization Organization (ISO) defines the framework and guidelines for LCA. The framework includes goal and scope definition, inventory analysis, impact assessment, and result interpretation [94,95]. The system boundary shall encompass all the activities associated with the collection and transportation of the crustacean shells to the biorefinery, processing, and conversion into nanostructured chitin.

Finally, techno-economic considerations are an integral part of defining the sustainability of a product. Process simulation models can help to estimate the material and energy balances of the process pathways producing nanostructured chitin using the process data from the experimental tasks. The economic analysis encompasses the estimation of the capital investment, operational expenses, and production costs.

4. Conclusions

This research introduces a sustainable and cost-effective method for producing nanochitin using inexpensive ionic liquids (ILs) such as $[HN_{222}][HSO_4]$, presenting a significant advancement over traditional chitin extraction processes. As mentioned in the introduction of this work, the applications to chitin nanowhiskers are broad, including packaging replacements, medical devices, and flexible electronics, to name but a few. Importantly for all the aforementioned applications, the IL reduces the overall production costs by simplifying the process, eliminating the need for initial purification steps, and reducing the consumption of chemicals and energy.

The scalability of this process promises broader implementation across sectors utilizing biopolymers. Future research should focus on further cost reductions for IL production and on evaluating the lifecycle impacts of these materials to enhance their commercial and environmental viability. This approach not only demonstrates a technological innovation in the production of chitin nanowhiskers but also exemplifies the application of green chemistry principles in materials science, setting a template for sustainable material production. The chitin nanowhiskers produced maintain high crystallinity and dimensional stability, making them suitable for various industrial applications including biomedicine, packaging, and electronics.

Supplementary Materials: The following supporting information can be downloaded at: https://www.mdpi.com/article/10.3390/suschem5020010/s1, Figure S1: General Scheme of preparation of ChNWs/Ch/ILs; Figure S2: First derivative of FTIR spectra of chitin and chitosan standards; Figure S3: Calibration curve for calculation of %DA; Figures S4–S6: Expanded FTIR spectra of chitin standard and chitin nanowhiskers (ChNWs) produced from chitin; Figures S7–S12: pXRD Peak Fitting (Origin); Figure S13: First derivative of FTIR spectra (1450–1150 cm^{-1}) of chitin standard and chitin nanowhiskers (ChNWs) produced from chitin; Table S1: Characteristic FTIR peaks identified in chitin samples reported in the literature; Tables S2–S7: Parameters of pXRD Peak Fitting (Origin); Table S8: Evaluation of crystallinity; Table S9: Evaluation of crystallite size; Table S10: MB1, MB2 and RB values elucidated from first derivative of FTIR spectra. References [96–98] are cited in Supplementary Materials.

Author Contributions: Conceptualization, J.L.S. and P.B.; methodology, J.L.S.; data collection and analysis, A.S.S., R.P.S. and J.L.S.; writing—original draft preparation, J.L.S. and P.B.; writing—review and editing, J.L.S., P.B. and O.T.; supervision, J.L.S.; funding acquisition, J.L.S. All authors have read and agreed to the published version of the manuscript.

Funding: This research was supported by NSF-I Corps 2243420 (prototype development funds).

Institutional Review Board Statement: Not applicable.

Informed Consent Statement: Not applicable.

Data Availability Statement: The original contributions presented in the study are included in the article/Supplementary Material; further inquiries can be directed to the corresponding authors.

Acknowledgments: The authors thank S.P. Kelley for the help with gypsum identification.

Conflicts of Interest: The authors declare no conflicts of interest.

References

1. Bai, L.; Liu, L.; Esquivel, M.; Tardy, B.L.; Huan, S.; Niu, X.; Liu, S.; Yang, G.; Fan, Y.; Rojas, O.J. Nanochitin: Chemistry, Structure, Assembly, and Applications. *Chem. Rev.* **2022**, *122*, 11604–11674. [CrossRef] [PubMed]
2. Li, J.; Revol, J.F.; Marchessault, R.H. Effect of degree of deacetylation of chitin on the properties of chitin crystallites. *J. Appl. Polym. Sci.* **1997**, *65*, 370–373. [CrossRef]
3. Foster, A.B.; Webber, J.M. Chitin. In *Advances in Carbohydrate Chemistry*; Melville, L., Wolfrom, R., Tipson, S., Eds.; Academic Press: Oxford, UK, 1961; pp. 371–393.
4. Visakh, P.M.; Thomas, S. Preparation of Bionanomaterials and Their Polymer Nanocomposites from Waste and Biomass. *Waste Biomass Valor.* **2010**, *1*, 121–134. [CrossRef]
5. Lee, S.; Hao, L.T.; Park, J.; Oh, D.X.; Hwang, D.S. Nanochitin and nanochitosan: Chitin nanostructure engineering with multiscale properties for biomedical and environmental applications. *Adv. Mater.* **2023**, *35*, e2203325. [CrossRef] [PubMed]
6. Vincent, J.F.V.; Wegst, U.G.K. Design and mechanical properties of insect cuticle. *Arthropod Struct. Dev.* **2004**, *33*, 187–199. [CrossRef] [PubMed]
7. Sanchez, C.; Boissiere, C.; Cassaignon, S.; Chaneac, C.; Durupthy, O.; Faustini, M.; Grosso, D.; Laberty-Robert, C.; Nicole, L.; Portehault, D.; et al. Molecular engineering of functional inorganic and hybrid materials. *Chem. Mater.* **2014**, *26*, 221–238. [CrossRef]
8. Dominic, C.D.M.; Joseph, R.; Sabura Begum, P.M.; Raghunandanan, A.; Vackkachan, N.T.; Padmanabhan, D.; Formela, K. Chitin nanowhiskers from shrimp shell waste as green filler in acrylonitrile-butadiene rubber: Processing and performance properties. *Carbohydr. Polym.* **2020**, *245*, 116505. [CrossRef] [PubMed]
9. Liu, Y.; Liu, M.; Yang, S.; Luo, B.; Zhou, C. Liquid crystalline behaviors of chitin nanocrystals and their reinforcing effect on natural rubber. *ACS Sustain. Chem. Eng.* **2018**, *6*, 325–336. [CrossRef]
10. Chi-Yan Li, S.; Sun, Y.C.; Guan, Q.; Naguib, H. Effects of chitin nanowhiskers on the thermal, barrier, mechanical, and rheological properties of polypropylene nanocomposites. *RSC Adv.* **2016**, *6*, 72086–72095. [CrossRef]
11. Wang, M.; Xue, H.; Feng, Z.; Cheng, B.; Yang, H. Increase of Tensile Strength and Toughness of Bio-Based Diglycidyl Ether of Bisphenol A with Chitin Nanowhiskers. *PLoS ONE* **2017**, *12*, e0177673. [CrossRef]
12. Rajak, D.K.; Pagar, D.D.; Kumar, R.; Pruncu, C.I. Recent progress of reinforcement materials: A comprehensive overview of composite materials. *J. Mater. Res. Technol.* **2019**, *8*, 6354–6374. [CrossRef]
13. Serventi, L.; He, Q.; Huang, J.; Mani, A.; Subhash, A.J. Advances in the preparations and applications of nanochitins. *Food Hydrocoll. Health* **2021**, *1*, 100036. [CrossRef]
14. Mushi, N.E.; Utsel, S.; Berglund, L.A. Nanostructured biocomposite films of high toughness based on native chitin nanofibers and chitosan. *Front. Chem.* **2014**, *2*, 99. [CrossRef] [PubMed]

15. Hashiguchi, T.; Yamamoto, K.; Kadokawa, J.-I. Fabrication of highly flexible nanochitin film and its composite film with anionic polysaccharide. *Carbohydr. Polym.* **2021**, *270*, 118369. [CrossRef] [PubMed]
16. Zhong, T.; Jian, G.; Chen, Z.; Wolcott, M.; Nassiri, S.; Fernandez, C.A. Interfacial interactions and reinforcing mechanisms of cellulose and chitin nanomaterials and starch derivatives for cement and concrete strength and durability enhancement: A review. *Nanotechnol. Rev.* **2022**, *11*, 2673–2713. [CrossRef]
17. Haider, M.M.; Jian, G.; Zhong, T.; Li, H.; Fernandez, C.A.; Fifield, L.S.; Wolcott, M.; Nassiri, S. Insights into setting time, rheological and mechanical properties of chitin nanocrystals- and chitin nanofibers-cement paste. *Cem. Concr. Compos.* **2022**, *132*, 104623. [CrossRef]
18. Fernandes, S.C.M.; Aguirre, G. Biopolymer micro/nanogel particles as smart drug delivery and theranostic systems. *Pharmaceutics* **2023**, *15*, 2060. [CrossRef] [PubMed]
19. Olza, S.; Salaberria, A.M.; Alonso-Varona, A.; Samanta, A.; Fernandes, S.C.M. The role of nanochitin in biologically-active matrices for tissue engineering–Where do we stand? *J. Mater. Chem. B* **2023**, *11*, 5630–5649. [CrossRef] [PubMed]
20. Zubillaga, V.; Salaberria, A.M.; Palomares, T.; Alonso-Varona, A.; Kootala, S.; Labidi, J.; Fernandes, S.C.M. Chitin nanoforms provide mechanical and topological cues to support growth of human adipose stem cells in chitosan matrices. *Biomacromolecules* **2018**, *19*, 3000–3012. [CrossRef]
21. Suneetha, M.; Kim, H.; Han, S.S. Doxorubicin-loaded fungal-carboxymethyl chitosan functionalized polydopamine nanoparticles for photothermal cancer therapy. *Pharmaceutics* **2023**, *15*, 1281. [CrossRef]
22. Dasan, Y.K.; Bhat, A.H.; Khan, I. 1. Nanocellulose and Nanochitin for Water Remediation by Adsorption of Heavy Metals. In *Nanomaterials for Water Remediation*; Kumar Mishra, A., Hussain, M.C., Mishra, S.B., Eds.; De Gruyter: Berlin, Germany; Boston, MA, USA, 2020; pp. 1–18. [CrossRef]
23. CORDIS: Functional Membranes/Filters with Anti/Low-Fouling Surfaces for Water Purification through Selective Adsorption on Biobased Nanocrystals and Fibrils. Available online: https://cordis.europa.eu/project/id/280519 (accessed on 12 February 2024).
24. Somasundaram, S.; Kumaravel, V. Application of Nanoparticles for Self-Cleaning Surfaces. In *Home Emerging Nanostructured Materials for Energy and Environmental Science*; Part of the Environmental Chemistry for a Sustainable World Book Series; Springer: Berlin/Heidelberg, Germany, 2019; Volume 23.
25. He, Y.; Lin, X.; Feng, Y.; Luo, B.; Liu, M. Carbon nanotube ink dispersed by chitin nanocrystals for thermoelectric converter for self-powering multifunctional wearable electronics. *Adv. Sci.* **2022**, *9*, e2204675. [CrossRef] [PubMed]
26. Schötz, S.; Reisbeck, F.; Schmitt, A.C.; Dimde, M.; Quaas, E.; Achazi, K.; Haag, R. Tunable polyglycerol-based redox-responsive nanogels for efficient cytochrome c delivery. *Pharmaceutics* **2021**, *13*, 1276. [CrossRef] [PubMed]
27. Andre, R.S.; dos Santos, D.M.; Mercante, L.A.; Facure, M.H.M.; Campana-Filho, S.P.; Mattoso, L.H.C.; Correa, D.S. Nanochitin-based composite films as a disposable ethanol sensor. *J. Environ. Chem. Eng.* **2020**, *8*, 104163. [CrossRef]
28. Heidarian, P.; Gharaie, S.; Yousefi, H.; Paulino, M.; Kaynak, A.; Varley, R.; Kouzani, A.Z.A. 3D printable dynamic nanocellulose/nanochitin self-healing hydrogel and soft strain sensor. *Carbohydr. Polym.* **2022**, *291*, 119545. [CrossRef] [PubMed]
29. Younes, I.; Rinaudo, M. Chitin and chitosan preparation from marine sources. Structure, properties and applications. *Mar. Drugs* **2015**, *13*, 1133–1174. [CrossRef] [PubMed]
30. Yang, N.; Xi, C. Sustainability: Don't waste seafood waste. *Nature* **2015**, *524*, 155–157. [CrossRef] [PubMed]
31. Chandrasekharan, M.; Sachindra, N.M.; Mahendrakar, N.S. Biotechnology for utilization of marine by-products. In *Fish Processing Byproducts*; Studium Press: Austin, TX, USA, 2015; pp. 43–62.
32. Poeloengasih, C.D.; Hernawan, D.; Angwarndo, M. Isolation and characterization of chitin and chitosan prepared under various processing times. *Indones. J. Chem.* **2008**, *8*, 189–192. [CrossRef]
33. Beaney, P.; Lizardi-Mendoza, J.; Healy, M. Comparison of chitins produced by chemical and bioprocessing methods. *J. Chem. Tech. Biotech.* **2005**, *80*, 145–150. [CrossRef]
34. Rinaudo, M. Chitin and chitosan: Properties and applications. *Prog. Polym. Sci.* **2006**, *31*, 603–632. [CrossRef]
35. Khoushab, F.; Yamabhai, M. Chitin Research Revisited. *Mar. Drugs* **2010**, *8*, 1988–2012. [CrossRef]
36. Joseph, B.; Sam, R.M.; Balakrishnan, P.; Maria, H.J.; Gopi, S.; Volova, T.; Fernandes, S.C.M.; Thomas, S. Extraction of nanochitin from marine resources and fabrication of polymer nanocomposites: Recent advances. *Polymers* **2020**, *12*, 1664. [CrossRef] [PubMed]
37. Druzian, S.P.; Zanatta, N.P.; Côrtes, L.N.; Fátima, A.; Streit, M. Preparation of chitin nanowhiskers and its application for crystal violet dye removal from wastewaters. *Environ. Sci. Pollut. Res.* **2019**, *26*, 28548–28557. [CrossRef] [PubMed]
38. Hong, S.; Yuan, Y.; Zhang, K.; Lian, H.; Liimatainen, H. Efficient Hydrolysis of Chitin in a Deep Eutectic Solvent Synergism for Production of Chitin Nanocrystals. *Nanomaterials* **2020**, *10*, 869. [CrossRef] [PubMed]
39. Yamamoto, Y.; Nishimura, T.; Saito, T.; Kato, T. $CaCO_3$/chitin-whisker hybrids: Formation of $CaCO_3$ crystals in chitin-based liquid-crystalline suspension. *Polym. J.* **2010**, *42*, 583–586. [CrossRef]
40. Revol, J.; Marchessaultf, R.H. In Vitro Chiral Nematic Ordering of Chitin Crystallites. *Int. J. Biol. Macromol.* **1993**, *15*, 329–335. [CrossRef] [PubMed]
41. Jin, T.; Liu, T.; Lam, E.; Moores, A. Chitin and chitosan on the nanoscale. *Nanoscale Horiz.* **2021**, *6*, 505–542. [CrossRef]
42. Li, Z.; Zhang, M.; Cheng, D.; Yang, R. Preparation of silver nano-particles immobilized onto chitin nano-crystals and their application to cellulose paper for imparting antimicrobial activity. *Carbohydr. Polym.* **2016**, *151*, 834–840. [CrossRef] [PubMed]

43. Fan, Y.; Saito, T.; Isogai, A. Chitin nanocrystals prepared by TEMPO-mediated oxidation of α-chitin. *Biomacromolecules* **2008**, *9*, 192–198. [CrossRef] [PubMed]
44. Salaberria, A.M.; Labidi, J.; Fernandes, S.C.M. Different routes to turn chitin into stunning nano-objects. *Eur. Polym. J.* **2015**, *68*, 503–515. [CrossRef]
45. Hou, C.; Zhang, J.; Zhang, X.; Wang, Y.; Li, T.; Xia, B.; Jiang, J.; Dong, W. High strength chitin nanocrystal/alginate filament prepared by wet-spinning in "green" coagulating bath. *Cellulose* **2022**, *29*, 8611–8621. [CrossRef]
46. Liu, P.; Liu, H.; Schäfer, T.; Gutmann, T.; Gibhardt, H.; Qi, H.; Tian, L.; Zhang, X.C.; Buntkowsky, G.; Zhang, K. Unexpected selective alkaline periodate oxidation of chitin for the isolation of chitin nanocrystals. *Green Chem.* **2021**, *23*, 745–751. [CrossRef]
47. Oun, A.A.; Rhim, J.W. Effect of Oxidized Chitin Nanocrystals Isolated by Ammonium Persulfate Method on the Properties of Carboxymethyl Cellulose-Based Films. *Carbohydr. Polym.* **2017**, *175*, 712–720. [CrossRef] [PubMed]
48. Li, Z.; Liu, C.; Hong, S.; Lian, H.; Mei, C.; Lee, J.; Wu, Q.; Hubbe, M.A.; Li, M. Recent Advances in Extraction and Processing of Chitin Using Deep Eutectic Solvents. *Chem. Eng. J.* **2022**, *446*, 136953. [CrossRef]
49. Berroci, M.; Vallejo, C.; Lizundia, E. Environmental impact assessment of chitin nanofibril and nanocrystal isolation from fungi, shrimp shells, and crab shells. *ACS Sustain. Chem. Eng.* **2022**, *10*, 14280–14293. [CrossRef]
50. Shamshina, J.L.; Abidi, N. Isolation of chitin nano-whiskers directly from crustacean biomass waste in a single step with acidic ionic liquid. *ACS Sustain. Chem. Eng.* **2022**, *10*, 11846–11855. [CrossRef]
51. Abidi, N.; Shamshina, J.L. Preparation of Chitin Nanocrystals and Nanowhiskers from Crustacean Biomass Using Ionic Liquid. WO2023059499A1, 29 September 2022. Available online: https://worldwide.espacenet.com/patent/search?q=PCT/US2022/045177 (accessed on 12 February 2024).
52. Singh, V.; Kaur, S.; Sapehiyia, V.; Singh, J.; Kad, G.L. Microwave accelerated preparation of [bmim][HSO_4] ionic liquid: An acid catalyst for improved synthesis of coumarins. *Catal. Commun.* **2005**, *6*, 57–60. [CrossRef]
53. Tao, D.-J.; Li, Z.-M.; Cheng, Z.; Hu, N.; Chen, X.-S. Kinetics study of the ketalization reaction of cyclohexanone with glycol using Brønsted acidic ionic liquids as catalysts. *Ind. Eng. Chem. Res.* **2012**, *51*, 16263–16269. [CrossRef]
54. Stocker, M.W.; Tsolaki, E.; Harding, M.J.; Healy, A.M.; Ferguson, S. Combining isolation-free and co-processing manufacturing approaches to access room temperature ionic liquid forms of APIs. *J. Pharm. Sci.* **2023**, *112*, 2079–2086. [CrossRef] [PubMed]
55. Alcalde, E.; Dinarès, I.; Ibáñez, A.; Mesquida, N. A Simple halide-to-anion exchange method for heteroaromatic salts and ionic liquids. *Molecules* **2012**, *17*, 4007–4027. [CrossRef]
56. Klein-Marcuschamer, D.; Simmons, B.A.; Blanch, H.W. Techno-economic analysis of a lignocellulosic ethanol biorefinery with ionic liquid pre-treatment. *Biofuels Bioprod. Bioref.* **2011**, *5*, 562–569. [CrossRef]
57. Chen, L.; Sharifzadeh, M.; Dowell, N.M.; Welton, T.; Shah, N.; Hallett, J.P. Inexpensive ionic liquids: $[HSO_4]^-$-based solvent production at bulk scale. *Green Chem.* **2014**, *16*, 3098–3106. [CrossRef]
58. George, A.; Brandt, A.; Tran, K.; Zahari, S.M.S.N.S.; Klein-Marcuschamer, D.; Sun, N.; Sathitsuksanoh, N.; Shi, J.; Stavila, V.; Parthasarathi, R.; et al. Design of low-cost ionic liquids for lignocellulosic biomass pretreatment. *Green Chem.* **2015**, *17*, 1728–1734. [CrossRef]
59. Zahari, S.M.S.N.S.; Azman, H.; Karim, L. Triethylammonium hydrogen sulfate ionic liquid as a low-cost solvent: A short review of synthesis, analysis and applications. In Proceedings of the MATEC Web conference, International Mechanical and Industrial Engineering Conference 2018 (IMIEC 2018), Malang, Indonesia, 30–31 August 2018; Volume 204. Available online: https://www.matec-conferences.org/articles/matecconf/abs/2018/63/matecconf_imiec2018_00006/matecconf_imiec2018_00006.html (accessed on 26 March 2024).
60. Brandt-Talbot, A.; Gschwend, F.J.V.; Fennell, P.S.; Lammens, T.M.; Tan, B.; Wealea, J.; Hallett, J.P. An economically viable ionic liquid for the fractionation of lignocellulosic biomass. *Green Chem.* **2017**, *19*, 3078. [CrossRef]
61. Karimi-Jaberi, Z.; Masoudi, B.; Rahmani, A.; Alborzi, K. Triethylammonium hydrogen sulfate [Et_3NH][HSO_4] as an efficient ionic liquid catalyst for the synthesis of coumarin derivatives. *Polycycl. Aromat. Compd.* **2020**, *40*, 99–107. [CrossRef]
62. Black, M.M.; Schwartz, H.M. The estimation of chitin and chitin nitrogen in crawfish waste and derived products. *Analyst* **1950**, *75*, 185–189. [CrossRef]
63. Scherrer, P. Determination of the size and internal structure of colloidal particles using X-rays. In *Kolloidchemie Ein Lehrbuch*; Springer: Berlin/Heidelberg, Germany, 1912; pp. 387–409.
64. Fan, Y.; Fukuzumi, H.; Saito, T.; Isogai, A. Comparative characterization of aqueous dispersions and cast films of different chitin nanowhiskers/nanofibers. *Int. J. Biol. Macromol.* **2012**, *50*, 69–76. [CrossRef] [PubMed]
65. Beil, S.; Schamberger, A.; Naumann, W.; Machill, S.; van Pee, K.-H. Determination of the degree of N-acetylation (DA) of chitin and chitosan in the presence of water by first derivative ATR FTIR spectroscopy. *Carbohydr. Polym.* **2012**, *87*, 117–122. [CrossRef] [PubMed]
66. PubChem. 1-Methylimidazolium (Compound). Available online: https://pubchem.ncbi.nlm.nih.gov/compound/1-Methylimidazolium#section=Synonyms (accessed on 6 April 2024).
67. Muckerman, J.T.; Skone, J.H.; Ning, M.; Wasada-Tsutsui, Y. Toward the accurate calculation of pKa values in water and acetonitrile. *Biochim. Biophys. Acta* **2013**, *1827*, 882–891. [CrossRef] [PubMed]
68. Grishina, E.P.; Ramenskaya, L.M.; Gruzdev, M.S.; Kraeva, O.V. Water effect on physicochemical properties of 1-butyl-3-methylimidazolium based ionic liquids with inorganic anions. *J. Mol. Liquids* **2013**, *177*, 267–272. Available online: https://www.sciencedirect.com/science/article/pii/S0167732212003819?via=ihub (accessed on 10 April 2024). [CrossRef]

69. Matuszek, K.; Chrobok, A.; Coleman, F.; Seddon, K.R.; Swadźba-Kwaśny, M. Tailoring ionic liquids: Structure, acidity and catalytic activity of a new class of protic ionic liquids based on oligomeric $[(HSO_4)_xH_{x-1}]$-anions. *Green Chem.* **2014**, *16*, 3463–3471. [CrossRef]
70. Belieres, J.P.; Angell, C.A. Protic ionic liquids: Preparation, characterization, and proton free energy level representation. *J. Phys. Chem. B* **2007**, *111*, 4926–4937. [CrossRef] [PubMed]
71. Zhang, X.; Mao, Y.; Schwab, N.; Briber, R. An efficient method for chitin processing using phosphoric acid: Oligomers, nanocrystals, and high polymers. In Proceedings of the APS March Meeting 2022, Chicago, IL, USA, 14–18 March 2022; abstract id.N00.094.
72. Muñoz-Núñez, C.; Fernández-García, M.; Muñoz-Bonilla, A. Chitin nanocrystals: Environmentally friendly materials for the development of bioactive films. *Coatings* **2022**, *12*, 144. [CrossRef]
73. Mincea, M.; Negrulescu, A.; Ostafe, V. Preparation, modification, and applications of chitin nanowhiskers: A review. ons of chitin nanowhiskers: A review. *Rev. Adv. Mater. Sci.* **2012**, *30*, 225–242.
74. Gómez Estaca, J.; Tovar, C.A.; Montero García, P.; Gómez Guillén, M.C. Structural, viscoelastic, and emulsifying properties of shrimp chitin nanowhisker dispersions as a function of acidic pHs. *J. Food Eng.* **2023**, *351*, 111519. [CrossRef]
75. Morin, A.; Dufresne, A. Nanocomposites of chitin whiskers from Riftia tubes and poly(caprolactone). *Macromolecules* **2002**, *35*, 22190–22199. [CrossRef]
76. Kumar, G.N.P.; Bhat, S.K. Preparation of chitin nano whiskers from mushrooms. *Int. J. Sci. Res. Publ.* **2018**, *8*, 130. [CrossRef]
77. Goodrich, J.D.; Winter, W.T. Alpha-chitin nanocrystals prepared from shrimp shells and their specific surface area measurement. *Biomacromolecules* **2007**, *8*, 252–255. [CrossRef] [PubMed]
78. Nguyen, H.V.D.; de Vries, R.; Stoyanov, S.D. Chitin nanowhiskers with improved properties obtained using natural deep eutectic solvent and mild mechanical processing. *Green Chem.* **2022**, *24*, 3834–3844. [CrossRef]
79. Abdul Haleem, M.; Parker, K.D. X-ray Diffraction Studies on the Structure of a Chitin. *Z. Naturforsch. C Biosci.* **1976**, *31*, 383–388. [CrossRef]
80. Focher, B.; Beltrame, P.L.; Naggi, A.; Torri, G. Alkaline N-deacetylation of chitin enhanced by flash treatments. Reaction kinetics and structure modifications. *Carbohydr. Polym.* **1990**, *12*, 405–418. [CrossRef]
81. Ioelovich, M. Crystallinity and hydrophility of chitin and chitosan. *Res. Rev. J. Chem.* **2014**, *3*, 7–14.
82. Osorio-Madrazo, A.; David, L.; Trombotto, S.; Lucas, J.-M.; Peniche-Covas, C.; Domard, A. Kinetics study of the solid-state acid hydrolysis of chitosan: Evolution of the crystallinity and macromolecular structure. *Biomacromolecules* **2010**, *11*, 1376–1386. [CrossRef] [PubMed]
83. Gupta, A.K.; Singhal, R.P. Carbon fibers prepared from tailored reversible-addition-fragmentation transfer copolymerization-derived poly(acrylonitrile)-co-poly(methylmethacrylate). *J. Polym. Sci. Polym. Phys. Ed.* **1983**, *21*, 2243–2262. [CrossRef]
84. Nansé, G.; Papirer, E.; Fioux, P.; Moguet, F.; Tressaud, A. Fluorination of carbon blacks: An X-ray photoelectron spectroscopy study: I. A literature review of XPS studies of fluorinated carbons. XPS investigation of some reference compounds. *Carbon* **1997**, *35*, 175–194. [CrossRef]
85. Pereira, A.G.; Muniz, E.C.; Hsieh, Y.L. Chitosan-sheath and chitin-core nanowhiskers. *Carbohydr. Polym.* **2014**, *107*, 158–166. [CrossRef] [PubMed]
86. Oun, A.A.; Rhim, J.W. Preparation of multifunctional chitin nanowhiskers/ZnO-Ag NPs and their effect on the properties of carboxymethyl cellulose-based nanocomposite film. *Carbohydr. Polym.* **2017**, *169*, 467–479. [CrossRef] [PubMed]
87. Böke, H.; Akkurt, S.; Özdemir, S.; Gökturk, E.H.; Saltik, E.N.C. Quantification of $CaCO_3$–$CaSO_3 \cdot 0.5H_2O$–$CaSO_4 \cdot 2H_2O$ mixtures by FTIR analysis and its ANN model. *Mater. Lett.* **2004**, *58*, 723–726. [CrossRef]
88. Al Dabbas, M.; Eisa, M.Y.; Kadhim, W.H. Estimation of gypsum-calcite percentages using a fourier transform infrared spectrophotometer (FTIR), in Alexandria Gypsiferous soil-Iraq. *Iraqi J. Sci.* **2014**, *55*, 1916–1926.
89. Morris, R.J. Infrared spectrophotometric analysis of calcium sulfate hydrates using internally standardized mineral oil mulls. *Anal. Chem.* **1963**, *35*, 1489–1492. [CrossRef]
90. RRUFF Data Base. Gypsum. Available online: https://rruff.info/gypsum/display=default/R040029 (accessed on 6 April 2024).
91. Kutschera, M.; Nicoleau, L.; Bräu, M. Nano-optimized Construction Materials by Nano-seeding and Crystallization Control. In *Nanotechnology in Civil Infrastructure*; Gopalakrishnan, K., Birgisson, B., Taylor, P., Attoh-Okine, N., Eds.; Springer: Berlin/Heidelberg, Germany, 2011; pp. 195–205. [CrossRef]
92. Shukla, J.; Mehta, M.J.; Kumar, A. Effect of ionic liquid additives on the solubility behavior and morphology of calcium sulfate dihydrate (gypsum) in the aqueous sodium chloride system and physicochemical solution properties at 30 °C. *J. Chem. Eng. Data* **2018**, *63*, 2743–2752. [CrossRef]
93. Moussout, H.; Ahlafi, H.; Aazza, M.; Bourakhouadar, M. Kinetics and mechanism of the thermal degradation of biopolymers chitin and chitosan using thermogravimetric analysis. *Polym. Degrad. Stab.* **2016**, *130*, 1–9. [CrossRef]
94. *ISO 14040*; Environmental Management, Life Cycle Assessment, Principles and Framework. ISO: Geneva, Switzerland, 2006. Available online: https://www.iso.org/standard/37456.html (accessed on 10 April 2024).
95. *ISO 14044*; Environmental Management, Life Cycle Assessment, Requirements and Guidelines. ISO: Geneva, Switzerland, 2006. Available online: https://www.iso.org/standard/38498.html (accessed on 10 April 2024).
96. Cárdenas, G.; Cabrera, G.; Taboada, E.; Miranda, S.P. Chitin characterization by SEM, FTIR, XRD, and ^{13}C cross polarization/mass angle spinning NMR. *J. Appl. Polym. Sci.* **2004**, 1876–1885. [CrossRef]

97. Kaya, M.; Mujtaba, M.; Ehrlich, H.; Salaberria, A.M.; Baran, T.; Amemiya, C.T.; Galli, R.; Akyuz, L.; Sargin, I.; Labidi, J. On chemistry of γ-chitin. *Carbohydr. Polym.* **2017**, *176*, 177–186. [CrossRef] [PubMed]
98. Akpan, E.I.; Gbenebor, O.P.; Adeosun, S.O. Synthesis and characterisation of chitin from periwinkle (*Tympanotonus fusatus* (L.)) and snail (*Lissachatina fulica* (Bowdich)) shells. *Int. J. Biol. Macromol.* **2018**, *106*, 1080–1088. [CrossRef]